

An Object-Based Approach for Detecting Small Brain Lesions: Application to Virchow-Robin Spaces

Xavier Descombes*, Frithjof Kruggel, Gert Wollny, and Hermann Josef Gertz

Abstract—This paper is concerned with the detection of multiple small brain lesions from magnetic resonance imaging (MRI) data. A model based on the marked point process framework is designed to detect Virchow-Robin spaces (VRSs). These tubular shaped spaces are due to retraction of the brain parenchyma from its supplying arteries. VRS are described by simple geometrical objects that are introduced as small tubular structures. Their radiometric properties are embedded in a data term. A prior model includes interactions describing the clustering property of VRS. A Reversible Jump Markov Chain Monte Carlo algorithm (RJMCMC) optimizes the proposed model, obtained by multiplying the prior and the data model. Example results are shown on T_1 -weighted MRI datasets of elderly subjects.

Index Terms—Features extraction, marked point processes, reversible jump MCMC, Virchow Robin spaces.

I. INTRODUCTION

DETECTING focal lesions in magnetic resonance imaging (MRI) data sets of the human head is considered a nontrivial segmentation task. Segmentation approaches require prior knowledge about the lesion characteristics (e.g., their expected compartment, size and shape, their signal statistics in relation to the embedding tissue), and thus, are generally targeted for detecting a specific lesion type (e.g., [6], [18], [24], and [29]). For historical reasons and their medical significance, most approaches focused on white matter (WM) lesions due to Multiple Sclerosis (e.g., [15], [19], [26]), while methods for segmenting large focal lesions appeared only recently (e.g., [13]).

Different types of small focal lesions are typically found in MRI scans of elderly subjects. Their neuropathological substrate and their influence on cognitive abilities is still under debate [10]. The neurobiological background of this work is to aid in discriminating healthy from pathological aging as revealed by MRI brain data sets.

While a trained human observer is still outperforming automatic approaches for lesion detection and discrimination, estimating the lesion count and describing their position is tedious

Manuscript received October 7, 2002; revised October 27, 2003. The work of X. Descombes was supported in part by the Max-Planck Institute (MPI) through a travel grant during summer 2001. The Associate Editor responsible for coordinating the review of this paper and recommending its publication was W. Niessen. Asterisk indicates corresponding author.

*X. Descombes is with Ariana, common project CNRS/INRIA/UNSA, INRIA, BP93, 2004 route des Lucioles, 06902 Sophia Antipolis Cedex, France (e-mail: xdescomb@sophia.inria.fr).

F. Kruggel and G. Wollny are with the Max-Planck Institute of Cognitive Neuroscience, 04103 Leipzig, Germany.

H. J. Gertz is with the Department of Psychiatry, University Clinic Leipzig, 04103 Leipzig, Germany.

Digital Object Identifier 10.1109/TMI.2003.823061

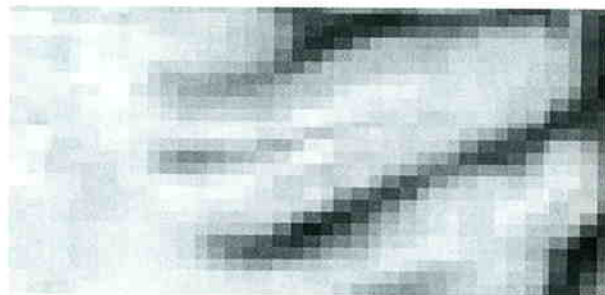


Fig. 1. An example of the tubular shape of VRS.

due to their multitude. So typically, these lesions are evaluated visually in the acquired data sets and rated by semiquantitative scales [22]. One such lesion type is called “enlarged Virchow-Robin space” (VRS) that corresponds to a small gap around a deep penetrating artery supplying the WM. Such lesions appear as small tubular structures filled with cerebro-spinal fluid (CSF) that are (ideally) radial to the brain surface. Typically, they are close to the spatial resolution limit of current MRI methods (1–3 mm in diameter and 3–15 mm long), and a single brain may contain hundreds of such lesions.

Herein, we consider an approach to detect small lesions that are nonuniformly distributed in space, have some shape prior and some constraints for their relative positions. Our framework is based on a marked point process and general under these hypotheses.

Structure and distribution of VRS have motivated the following approach. First, a VRS typically consists of several voxels forming a tubular shape (see Fig. 1). Thus, an approach based on a geometrical object appears suited for this problem. Second, VRS are not uniformly localized and some regionally higher occurrence can be observed (see Fig. 2). Interactions between objects are included in the model to favor clustering of VRS while suppressing an overlap of different VRS. A certain shape variability (length and diameter of the tubular structures in our case) and data noise have to be taken into account introducing local minima of the model-related cost function. To overcome this problem, we consider a stochastic framework.

The template theory introduced by Grenander allows modeling random shapes [9]. Within this pattern theory framework, several kinds of objects can be considered and complex scenes containing several objects can be represented by a graph [17]. In our context, the object’s shape model is simple and represented by a small segment. The complexity of the model lies in the different object interactions we will introduce. Therefore, we have preferred the marked point process framework here [1], [2]. This framework has been successfully applied in image analysis, e.g.,

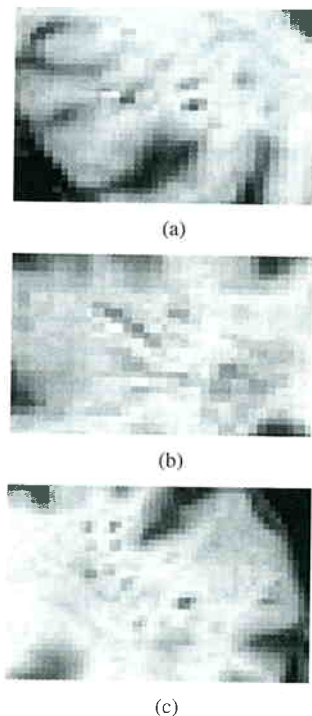


Fig. 2. An example of the clustering property of VRS: (a) axial, (b) coronal, and (c) sagittal sections.

in the context of cell segmentation [14], [21] or road network extraction [23]. A point process with a Poisson density measure models the number of objects and their localization in the scene. This process may include interactions between points such as explicit relations or clustering properties. Shape parameters are associated with the points to define the object geometry (e.g., length and orientation of an object).

Model optimization can be achieved by a birth and death process [2], a jump diffusion [17] or a Reversible Jump Markov Chain Monte Carlo algorithm (RJCMC) [5], [8]. Birth and death processes require the computation of a birth (or death) rate map which leads to costly algorithms on a three-dimensional (3-D) volume. The main advantage of the RJCMC approach lies in the flexibility of the derived algorithms. Within this framework, we can define dynamics adapted to the target distribution. Therefore, we prefer a RJCMC algorithm embedded in a simulated annealing scheme. We define a proposition kernel mixing different subkernels allowing us to move or to add and suppress objects. Some specific subkernels allow us to speed up the convergence rate of the algorithm.

In the Section II, we describe a data model for VRS. Filters designed as VRS indicators define the space where the first points of the objects are located. The subsequent section introduces the marked point process that consists of the prior model

(i.e., the geometry of the object and their interactions) and the data term (i.e., the filter output). The RJCMC algorithm is described in Section IV. Section V is devoted to results. Finally, some conclusions are drawn in Section VI.

II. DATA MODEL

In this section, we derive filters which can be interpreted as VRS indicators. These filters extract the information provided by the radiometry (grey level of voxels). However, this information is not sufficient to characterize the lesion, so a prior is defined to include knowledge about the relative localization and geometric properties of VRS. Filter results serve to define the data term and the volume where the point of the process defined in Section III are living. In a first approach, they can be modeled as small tubular structures, with a diameter close to the data resolution (typically 1–3 mm, [3]). Their length varies with an average of 3–4 mm but can reach up to 15 mm in exceptional cases. The data representation of these structures is discrete due to the discrete nature of the image lattice. The induced discretization is far from being isotropic. Therefore, we can only consider the three main directions (u, v, w) defined by the data without losing significant information. For these three directions we design filters that take the diameter variability and the partial volume effect into account. A filter lies in the plane perpendicular to the considered direction, say u . It consists of a central voxel s , the eight surrounding neighbors $t_1 \in \mathcal{N}_u^1(s)$, and the next 16 neighbors $t_2 \in \mathcal{N}_u^2(s)$ (see Fig. 4). A VRS is characterized by three properties: 1) VRS contain CSF that should appear as low-intensity voxels in T_1 -weighted datasets. 2) Surrounding tissue (i.e., WM or GM voxels) may increase lesion intensities due to the partial volume effect. Thus, neighboring voxels will have higher intensity and 3) are contrasted with the VRS voxels. We define three filters corresponding to these three properties $F^{\text{black}}(i_s)$, $F^{\text{white}}(\min(i_t, t \in \mathcal{N}_u^2(s)))$ and $F^{\text{contrast}}(\sum_{t \in \mathcal{N}_u^2(s)} i_t / 16)$, where i_s represents the grey level of voxel s in the data. Note that these three properties are not equivalent. Considering only one of them leads to false alarms in the CSF compartment for property 1), in the WM for property 2), and in the thin GM structures for property 3). The three defined functions depend on the data statistics and are defined on Fig. 3. We combine these three properties as shown in (1) at the bottom of the page. To avoid multiple detections of the same VRS, the final filter is written as follows:

$$F_u(s) = \begin{cases} f_u(s), & \text{if } \forall t \in \mathcal{N}_u^1(s), i_s \leq i_t \\ \min(0, f_u(s)), & \text{otherwise} \end{cases} \quad (2)$$

To compute the mean and standard deviation of the CSF, GM, and WM, we used a segmentation based on a region growing

$$f_u(s) = \min \left(F^{\text{black}}(i_s), F^{\text{white}}(\min(i_t, t \in \mathcal{N}_u^2(s))), F^{\text{contrast}} \left(\frac{\sum_{t \in \mathcal{N}_u^2(s)} i_t}{16} \right) \right). \quad (1)$$

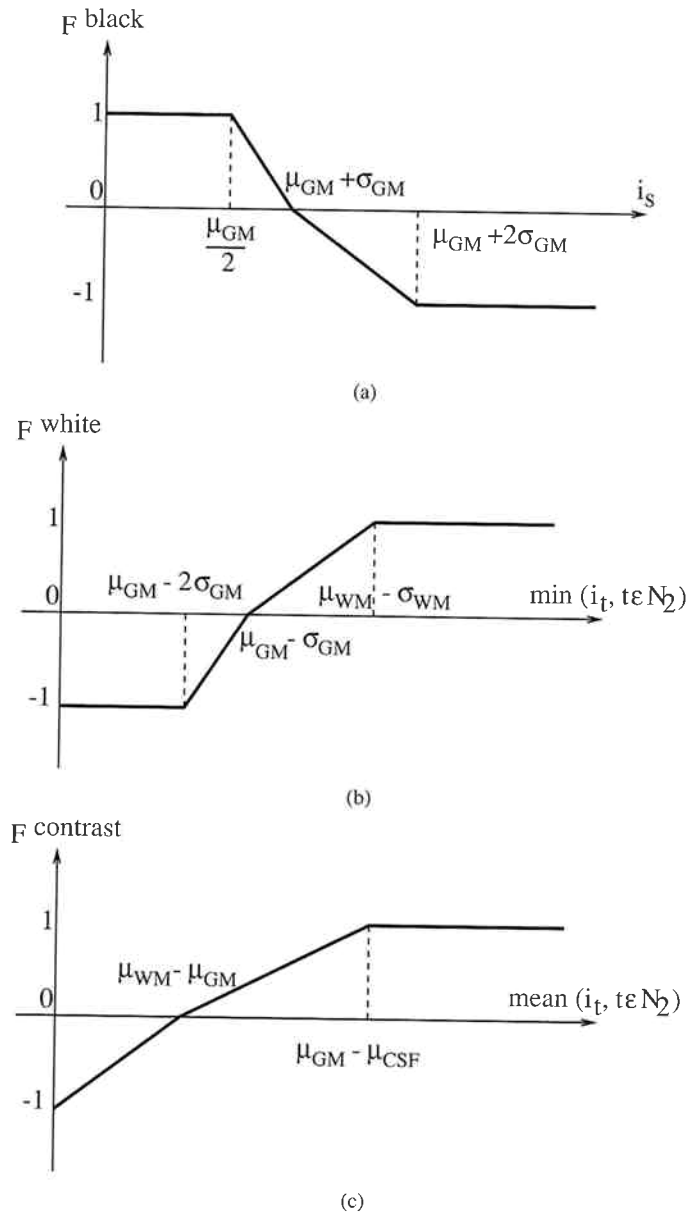


Fig. 3. The three filters characterizing VRS data: μ_{CSF} , μ_{GM} , and μ_{WM} represent the mean of CSF, GM, and WM, σ_x being the associated standard deviations.

approach [12]. The presence of lesions leads to local segmentation errors. Since their total volume is small [13], we neglect this influence on the grey level statistics of the different classes.

III. THE MARKED POINT PROCESS

To increase the sensitivity and reduce the false alarms rate, we have to consider geometric information about VRS. Besides, VRS are not distributed uniformly in the brain. The information on their location obtained from medical studies has to be considered. The marked point process framework is adapted here because it can embed such properties. The number of objects is random (we do not know *a priori* the number of VRS in a dataset), some prior knowledge concerning the geometry is modeled by the object definition and by a density on the underlying parameters. Besides, some interactions between objects

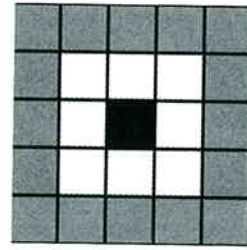


Fig. 4. VRS indicator filter: central voxel s in black, first neighborhood $\mathcal{N}_u^1(s)$ in white, and second neighborhood $\mathcal{N}_u^2(s)$ in grey.

allow us to take into account the information concerning the localization and the relations between the different VRS.

The full model $h(x)$ for the marked point process consists of the prior model $f(x)$ and the data term $g(x)$

$$h(x) = f(x)g(x). \quad (3)$$

Both terms are now discussed in detail.

A. Prior Model

The prior model takes the geometry of a detected object and its interactions into account. Each object is represented by a point with attributes (or marks) that define its geometry. The resulting configurations is a set of marked points $x = \{s(1) = (x(1), l(1)), \dots, s(n) = (x(n), l(n))\}$ where $x(i) \in V$ and $l(i)$ is a vector in \mathcal{R}^3 . We restrict the volume V to the space of points that satisfy $\max(F_u(x(i)), F_v(x(i)), F_w(x(i))) \geq 0$, where F_u , F_v and F_w are the filters defined in Section II.

We consider objects as small oriented segments \vec{s} with ending points x and $x + \vec{l}$ where $x \in V$ and $\|\vec{l}\| \in [\rho_{\min}, \rho_{\max}]$, ρ_{\min} (ρ_{\max}) corresponds to the minimum (maximum) segment length. We define a distribution on the configuration space whose density with respect to a Poisson measure is written as follows:

$$f(x) \propto \beta^n \prod_{k \in \{1, n\}} q_1(\|\vec{l}(k)\|) \prod_{k, k' \in \{1, n\}: k \sim k'} q_2(\vec{s}(k), \vec{s}(k')) \quad (4)$$

where \sim defines a neighborhood relation. β is a density parameter which drives the number of objects in the configuration (note that the density $f(x) \propto \beta^n$ corresponds to a Poisson process with intensity β). The term $q_1(\|\vec{l}(k)\|)$ represents a prior on the segment length and is defined as follows:

$$q_1(\|\vec{l}(k)\|) = \exp - \left[A \left(\frac{\rho_{\max} - \|\vec{l}(k)\|}{\rho_{\max} - \rho_{\min}} \right)^2 \right]. \quad (5)$$

In our experiments, we have chosen $\rho_{\min} = 2$ and $\rho_{\max} = 15$, according to the length of VRS observed in our datasets and reported in the literature [10], [11]. The term $q_2(\vec{s}(k), \vec{s}(k'))$ defines interactions between neighboring segments. We consider three kinds of interactions (see Fig. 5): 1) an explicit term which penalizes intersecting segments; 2) a clustering term which favors neighboring segments with similar orientation; and 3) a repulsive term which penalizes neighboring segments